

Subgap tunneling by a quantum interference effect with a collective channel: charge density waves in connection with insulators and crossed transport in superconductors

S. Duhot and R. Mélin

Institut NEEL, CNRS & Université Joseph Fourier, BP 166, F-38042 Grenoble Cedex 9

A quantum interference effect having the phenomenology of weak localization is discussed for subgap tunneling over a distance comparable to the coherence length, which is a consequence of “advanced-advanced” and “retarded-retarded” transmission modes [Altland and Zirnbauer, Phys. Rev. B **55**, 1142 (1997)]. Effects typical of disorder are obtained from the interplay between multichannel averaging and higher order processes in the tunnel amplitudes. We contrast weak localization-like subgap tunneling with a collective channel in three related gapped systems:

i) Momentum transfers similar to CDW Andreev processes propagate across a quasi-one dimensional band insulator for weak localization-like subgap tunneling in a peculiar type of *normal tunnel junction* without extrinsic CDW pairing. The “collective” channel corresponds in this case to a recoil of the insulating part of the junction.

ii) Weak localization-like subgap tunneling involves a collective channel with long distance propagation of a pair in the condensate for *crossed transport in three terminal superconducting hybrids* in trilayer geometries, which couples to a phase gradient due to a supercurrent in the superconducting electrode.

iii) Quantum interference effects similar to i) explain *magnetoresistance oscillations of a CDW pierced by nanoholes* [Latyshev *et al.*, Phys. Rev. Lett. **78**, 919 (1997)], which is the main result of the paper. Subgap tunneling is coupled to the sliding motion by charge accumulation in the interrupted chains. The effect is within the same trend as random matrix theory for normal metal-CDW hybrids [Visscher *et al.*, Phys. Rev. B **62**, 6873 (2000)]. We show that iii) resembles i) rather than ii), and that iii) is thus not a probe of the CDW quantum mechanical ground state.

PACS numbers: 73.20.Fz, 73.23.-b, 71.45.Lr, 74.78.Na

I. INTRODUCTION

Normal electron tunneling¹ through a barrier is realized in two-terminal devices at the tip of a scanning tunneling microscope, or by extended interfaces for planar tunnel junctions. Diffusive conductors can be described by arrays of tunnel junctions^{2,3} and it is desirable to develop a thorough understanding of all aspects of weak localization already at the level of a single tunnel junction. Starting from a model system of normal electrons tunneling through a band insulator (with hypothesis on the dimensionality and on the extrema of the dispersion relation), we investigate in our article the same weak localization-like tunneling mechanism^{4,5} in related systems: superconductors and charge density waves (CDWs). As shown from microscopic theory, a coupling to a collective channel is involved for weak localization-like subgap tunneling in each of the three cases. Moreover, weak localization-like subgap tunneling is the clue to an experiment by Latyshev *et al.*⁶ on $h/2e$ oscillations of the CDW motion around a nanohole of size comparable to the CDW coherence length.

CDWs realize a well known phase of quasi-one dimensional (quasi-1D) conductors⁷, with density modulations along the direction of the chains in the ground state, with a gap and a collective sliding motion above the depinning threshold. CDWs can be nano-fabricated, as shown by various experiments in the last decade^{8,9,10,11,12}.

We show that weak localization-like tunneling discussed below appears already in a specific type of tunnel

junction. In this case, $h/2e$ modulations of the tunneling current as a function of the applied magnetic flux require a coupling to an additional momentum channel in parallel to evanescent wave charge tunneling. This channel corresponds to a recoil of the insulator with $2k_F$ transfers of momentum (k_F is the Fermi wave-vector) propagating across the insulator, from one interface to the other. Such transfers of momentum occur also in CDW Andreev reflection^{12,13,14}, which raises naturally the question of a common effect of weak localization-like tunneling in band insulators and CDWs. This leads to an interpretation of the experiment by Latyshev *et al.*⁶ on $h/2e$ oscillations of the charge density wave motion around nanoholes. A film of the CDW compound NbSe_3 pierced by the nanoholes formed by columnar defects was obtained from ion irradiation by Latyshev *et al.*⁶, and the experimental results were reproduced after publication. The diameter $D \simeq 10 \text{ nm}$ of the nanohole is comparable to the ballistic CDW coherence length $\xi_0 = \hbar v_F / \Delta$, with v_F the Fermi velocity and Δ the Peierls gap of the CDW⁶. We reach an agreement with the following experimental observations⁶ for the (un)irradiated sample (not) containing nanoholes: 1. Absence of magnetoresistance oscillations without nanoholes; 2. Absence of magnetoresistance oscillations with nanoholes but without sliding motion; 3. $h/2e$ oscillations of the resistance as a function of magnetic flux with nanoholes and with sliding motion; 4. Positive magnetoresistance at low fields with nanoholes; 5. Oscillations at temperature as high as $\simeq 52\text{K}$ with nanoholes.

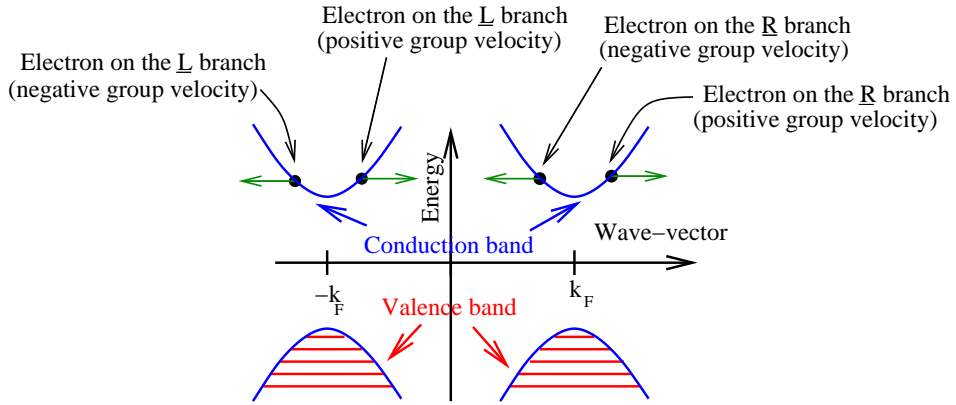


FIG. 1: (Color online.) Schematic representation of the BCS-like dispersion relation of the band insulator with a gap Δ . All states are populated by genuine electrons and holes, resulting in a band insulator, not in a superconductor. Electrons with wave-vectors $\pm k_F$ are labeled by R and L . A R electron can have a positive or negative group velocities, as shown on the figure.

Previous approaches to related phenomena in CDWs were based on weak localization in normal metal-CDW hybrids in the framework of random matrix theory¹⁵, Aharonov-Bohm oscillations¹⁶, soliton tunneling^{16,17} and permanent currents^{18,19}. The effect that we consider is not directly related to non linearities of the CDW phase Hamiltonian^{20,21,22,23,24,25,26,27,28,29,30,31,32,33}. We reach consistency with Visscher *et al.*¹⁵ finding on the basis of random matrix theory an unexpected strong effect of weak localization for CDWs connected to a disordered normal electrode.

Concerning now the related issue of tunneling through superconductors, three-terminal^{34,35} configurations allow part of the tunneling current to be converted as an electronic collective supercurrent because of “crossed Andreev reflection”^{36,37,38,39,40,41,42,43,44,45}, corresponding to the emission of a pair by a tunneling electron. The later is then transmitted as a hole in another electrode. Unexpected experimental results were obtained recently for “crossed transport” (subgap tunneling in a three terminal configuration) in normal metal - superconductor - normal metal trilayers by Russo *et al.*⁴⁶ or in ferromagnet - superconductor - ferromagnet structures with lateral contacts by Beckmann *et al.*⁴⁷, as well as more recently by Cadden-Zimansky and Chandrasekhar⁴⁸. In these experiments related to the realization of a source of entangled pairs of electrons^{49,50}, the distance L separating both interfaces between the normal (or ferromagnetic) metals and the superconductor is approximately larger than the coherence length ξ_0 . The effects discussed below rely on a geometrical parameter being comparable to the coherence length, either $L \gtrsim \xi_0$ for a superconductor, or $D \sim \xi_0$ for a nanohole of diameter D in a CDW film.

Non standard localization effects were already introduced in superconducting hybrid structures by Altland and Zirnbauer for an Andreev quantum dot⁵¹, who state at the end of their abstract that in normal metal-

superconductor hybrids, “*every Cooperon and diffusion mode in the advanced-retarded channel entails a corresponding mode in the advanced-advanced (or retarded-retarded) channel*”, which constitutes the technical basis of our discussion where “diffusion modes” become “transmission modes”.

The structure of the article is as follows. Preliminaries are presented in Sec. II. Sec. III is logically focused on obtaining related results for band insulators (Sec. III A) and superconductors (Sec. III B). Sec. IV presents our results on charge density waves in connection with Sec. III and with the experiments by Latyshev *et al.*⁶. Concluding remarks are presented in Sec. V. The discussion in the main body of the article is complemented by two Appendices.

II. PRELIMINARIES: HAMILTONIANS, GREEN'S FUNCTIONS, WEAK LOCALIZATION LOOPS

We start with necessary preliminaries on the microscopic description. Insulators (Sec. II A), superconductors (Sec. II B) and charge density waves (Sec. II C) are described by the same formalism. Weak localization-like subgap tunneling is introduced in Sec. II D.

A. Description of a band insulator

We consider for the band insulator the same dispersion relation as for the BCS model (see Fig. 1), and assume excitation branches supporting either electrons or holes, without condensate and without explicit CDW or superconducting symmetry breaking.

The advanced Green's function connecting two sites α

and β separated by a distance $R_{\alpha,\beta}$ is given by

$$g_{\alpha,\beta}^A(\omega) = \frac{\pi\rho_N}{k_F|R_{\alpha,\beta}|} \sin(k_F|R_{\alpha,\beta}|) \times \frac{-\hbar\omega}{\sqrt{|\Delta|^2 - (\hbar\omega)^2}} \exp(-|R_{\alpha,\beta}|/\xi(\omega)), \quad (1)$$

where ρ_N is the normal density of states, k_F the Fermi wave-vector corresponding to the extrema of the dispersion relation, and $\xi(\omega) = \hbar v_F / \sqrt{|\Delta|^2 - (\hbar\omega)^2}$ the coherence length at energy $\hbar\omega$, with v_F the Fermi velocity.

Propagation across the insulator is supposed to be quasi-1D (see the discussion in the forthcoming Sec. III A 2), and we separate right (label R) from left (label L) branches (underlines are used to avoid confusion with the “A” and “R” labels for advanced and retarded Green’s functions) having a wave-vector $\simeq \pm k_F$. An electron on the R branch can have a positive or negative group velocity (see Fig. 1). The corresponding 2×2 matrix Green’s function between times t and t' and positions α and β are given by⁵²

$$\hat{g}_{\alpha,\beta}^A(t, t') = -i\theta(t - t') \times \begin{bmatrix} \langle \{c_{\alpha,\underline{R}}^+(t'), c_{\beta,\underline{R}}(t)\} \rangle & \langle \{c_{\alpha,\underline{R}}^+(t'), c_{\beta,\underline{L}}(t)\} \rangle \\ \langle \{c_{\alpha,\underline{L}}^+(t'), c_{\beta,\underline{R}}(t)\} \rangle & \langle \{c_{\alpha,\underline{L}}^+(t'), c_{\beta,\underline{L}}(t)\} \rangle \end{bmatrix}. \quad (2)$$

Eq. (2) reduces to

$$\hat{g}_{\alpha,\beta}^A(\omega) = \pi\rho_N \frac{-\hbar\omega}{\sqrt{|\Delta|^2 - (\hbar\omega)^2}} \exp(-|R_{\alpha,\beta}|/\xi) \quad (3)$$

$$\times \begin{bmatrix} \exp(i k_F R_{\alpha,\beta}) & 0 \\ 0 & \exp(-i k_F R_{\alpha,\beta}) \end{bmatrix}$$

for propagation at energy $\hbar\omega$ between two points separated by $R_{\alpha,\beta}$ along a given chain. Eq. (3) in 1D is compatible with Eq. (1) in 3D because the $\sin(k_F|R_{\alpha,\beta}|)/k_F|R_{\alpha,\beta}|$ factor in 3D is replaced by $\cos(k_F R_{\alpha,\beta})$ in 1D.

B. Description of a superconductor

1. BCS Hamiltonian

Superconductors are described by the BCS Hamiltonian

$$\mathcal{H}_{\text{BCS}} = \sum_{\langle\alpha,\beta\rangle,\sigma} -T \left(c_{\alpha,\sigma}^+ c_{\beta,\sigma} + c_{\beta,\sigma}^+ c_{\alpha,\sigma} \right) \quad (4)$$

$$+ \sum_{\alpha} \left(\Delta c_{\alpha,\uparrow}^+ c_{\alpha,\downarrow}^+ + \Delta^* c_{\alpha,\downarrow} c_{\alpha,\uparrow} \right),$$

where we suppose a bulk hopping amplitude T , where $\langle\alpha,\beta\rangle$ label neighboring sites on a cubic lattice with a lattice parameter a_0 , and Δ^* is the complex conjugate of the gap Δ . Spin- σ electrons destroyed at site α are

created at the neighboring site β under the action of $c_{\beta,\sigma}^+ c_{\alpha,\sigma}$. Propagation in the bulk of the superconductor is described by Eq. (4) at low filling, with a kinetic energy $\xi_k = \hbar^2 k^2 / 2m - \mu$ with respect to the chemical potential μ , and with m the band mass.

2. Ballistic Green’s functions

The ballistic advanced Nambu Green’s function of a superconductor is defined by

$$\hat{g}_{\alpha,\beta}^A(t, t') = -i\theta(t - t') \times \begin{bmatrix} \langle \{c_{\alpha,\uparrow}^+(t'), c_{\beta,\uparrow}(t)\} \rangle & \langle \{c_{\alpha,\downarrow}^+(t'), c_{\beta,\uparrow}(t)\} \rangle \\ \langle \{c_{\alpha,\downarrow}(t'), c_{\beta,\uparrow}(t)\} \rangle & \langle \{c_{\alpha,\downarrow}(t'), c_{\beta,\downarrow}^+(t)\} \rangle \end{bmatrix}, \quad (5)$$

where the entries correspond to electrons and holes. Spin rotational invariance is assumed, and therefore we use 2×2 Green’s functions in the spin sector $S_z = \pm \hbar/2$. The advanced Green’s function connecting two points labeled by α and β , and separated by a distance $R_{\alpha,\beta}$ at energy $\hbar\omega$ takes the form^{38,39,53}

$$\hat{g}(R_{\alpha,\beta}, \omega) = \begin{bmatrix} g_+(R_{\alpha,\beta}, \omega) & f(R_{\alpha,\beta}, \omega) \\ f(R_{\alpha,\beta}, \omega) & g_-(R_{\alpha,\beta}, \omega) \end{bmatrix}, \quad (6)$$

with

$$g_{\pm}(R_{\alpha,\beta}, \omega) = \pi\rho_N \exp\left(-\frac{R_{\alpha,\beta}}{\xi(\omega)}\right) \quad (7)$$

$$\times \left\{ \sin(k_F R_{\alpha,\beta}) \frac{-\hbar\omega}{\sqrt{|\Delta|^2 - (\hbar\omega)^2}} \mp \cos(k_F R_{\alpha,\beta}) \right\}$$

$$f(R_{\alpha,\beta}, \omega) = \pi\rho_N \exp\left(-\frac{R_{\alpha,\beta}}{\xi(\omega)}\right) \quad (8)$$

$$\times \sin(k_F R_{\alpha,\beta}) \frac{\Delta}{\sqrt{|\Delta|^2 - (\hbar\omega)^2}},$$

where ρ_N is the normal density of states and $\xi(\omega) = \hbar v_F / \sqrt{|\Delta|^2 - (\hbar\omega)^2}$ is the coherence length at energy $\hbar\omega$, with v_F the Fermi velocity.

C. Description of a charge density wave

1. Peierls Hamiltonian

Charge density waves are described on the basis of the electronic part of the Peierls Hamiltonian of spinless fermions on a 1D chain:

$$\mathcal{H}_P = - \sum_x [T + \delta_0 \cos(2k_F x)] [c_{x+a_0}^+ c_x + c_x^+ c_{x+a_0}], \quad (9)$$

where the average hopping amplitude T has a modulation δ_0 (a_0 is the lattice parameter). Changing variable from

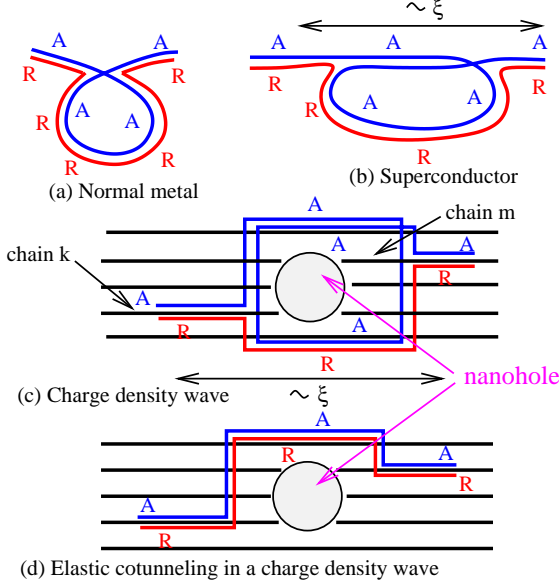


FIG. 2: (Color online.) Schematic representation in real space of a localization loop inserted in diagrams for the transmission coefficient in a normal metal (a); and in a superconductor^{4,5} (b). Similar diagrams are obtained from the tunnel terms at the interfaces⁴ to higher orders (see Sec. III B). (c) shows a weak localization-like loop for a quasi-1D charge density wave chains pierced by a nanohole (see Sec. IV). (d) shows an elastic cotunneling process (see Sec. IV C), not modulated by the magnetic flux. The labels “A” and “R” stand for advanced and retarded Green’s functions.

the spatial coordinate x along the chain to the wavevector k , we find

$$\mathcal{H} = - \sum_k 2T \cos(ka_0) c_k^+ c_k - \sum_k \Delta c_{k-2k_F}^+ c_k - \sum_k \Delta^* c_{k+2k_F}^+ c_k, \quad (10)$$

with $|\Delta| = \delta_0$ the Peierls gap.

2. Ballistic Green’s functions

Ballistic propagation within a given CDW chain is described by Eq. (2). The CDW counterpart of Eq. (6) takes the form

$$\hat{g}_{\alpha,\beta}^A(\omega) = \begin{bmatrix} A & B \\ C & D \end{bmatrix}, \quad (11)$$

with

$$A = g_0(\omega) \exp(ik_F(x_\alpha - x_\beta)) \quad (12)$$

$$B = f_0(\omega) \exp(ik_F(x_\alpha + x_\beta)) \quad (13)$$

$$C = f_0(\omega) \exp(-ik_F(x_\alpha + x_\beta)) \quad (14)$$

$$D = g_0(\omega) \exp(-ik_F(x_\alpha - x_\beta)), \quad (15)$$

where the points α and β are at coordinates x_α and x_β along the chains, and where

$$g_0(\omega) = \frac{1}{4T} \left(\frac{-\hbar\omega}{\sqrt{|\Delta|^2 - (\hbar\omega)^2}} + i \right) \quad (16)$$

$$f_0(\omega) = \frac{1}{4T} \frac{\Delta}{\sqrt{|\Delta|^2 - (\hbar\omega)^2}}. \quad (17)$$

3. Tunneling self-energy

One dimensional chains with an average intra-chain hopping T are supposed to be connected by a weak interchain hopping t_\perp . The later corresponds to $c_{\alpha,R}^+$, encoding the destruction of a spinless fermion at site “a” and its creation at site α in a neighboring chain, as well as to the reversed process. The fermion creation operator c_a^+ is decomposed in the right (R)- and left (L)-moving components $c_{a,R}^+$ and $c_{a,L}^+$ according to

$$c_a^+ = \frac{1}{\sqrt{2}} (c_{a,R}^+ + c_{a,L}^+), \quad (18)$$

with $c_{a,R}^+ = e^{ik_F x_a} \hat{\chi}_R^+(x_a)$ and $c_{a,L}^+ = e^{-ik_F x_a} \hat{\chi}_L^+(x_a)$ (site “a” is at coordinate x_a along the chain). The fields $\hat{\chi}_{R(L)}^+(x)$ are slowly varying as a function of the coordinate x along the chain. The identity

$$c_a^+ c_\alpha = \frac{1}{2} (c_{a,L}^+ c_{\alpha,L}^- + c_{a,R}^+ c_{\alpha,R}^- + c_{a,L}^+ c_{\alpha,R}^- + c_{a,R}^+ c_{\alpha,L}^-) \quad (19)$$

leads to the self-energy

$$\hat{\Sigma}_{\alpha \rightarrow a}^A = \frac{t_\perp}{2} \begin{bmatrix} 1 & 1 \\ 1 & 1 \end{bmatrix} \quad (20)$$

for hopping from α to a , where the entries correspond to different left and right components.

D. Weak localization-like loops

A weak localization loop in a normal metal is shown on Fig. 2a. The generalization to subgap transport⁵ involves a Hikami box^{54,55} containing an “advanced-advanced” or a “retarded-retarded” transmission mode⁵¹. Fig. 2b shows a weak localization-like diffuson self-crossing in the bulk of the superconductor, and the same type of diagram from higher order terms in the tunnel amplitudes in normal metal - insulator - normal (NIN) metal and normal metal - insulator - superconductor - insulator - normal metal (NISIN) structures are discussed in the forthcoming Sec. III. The generalization to a quasi-1D CDW (see Sec. IV) corresponds to Fig. 2c, and a process of elastic cotunneling in a CDW is shown on Fig. 2d. The later is not modulated by a magnetic field because the magnetic field phase factor accumulated by the “advanced” and “retarded” Green’s functions cancel with each other in the diagram on Fig. 2d.

III. TUNNELING THROUGH A BAND INSULATOR AND CROSSED TRANSPORT IN SUPERCONDUCTING HYBRIDS

A. Subgap tunneling by a quantum interference effect in a normal tunnel junction

We start with a tunnel junction consisting of a band insulator inserted in between two normal electrodes. The assumption on the dispersion relation (see Fig. 3 and Sec. II A) is representative of extrema of the dispersion relation at wave-vectors p_n , with $2\pi/p_n$ much smaller than the thickness of the insulating layer traversed by tunneling electrons. Sec. III A 1 and Appendix A present expansions of the exact transport formula¹ in a ring geometry and for planar interfaces respectively, both leading to weak localization-like diagrams resembling Figs. 2b and c. The issue of the momentum transferred across the insulator is discussed in Sec. III A 2.

1. Ring geometry

a. Transport formula: We start with the Caroli, Combescot, Nozières and Saint James¹ expression of the conductance $\mathcal{G}(\omega)$ of a 1D NaIN_b junction:

$$\begin{aligned} \mathcal{G}(\omega) = & \quad (21) \\ 4\pi^2 \frac{e^2}{h} \rho_{a,a}(\omega) t_{a,\alpha} G_{\alpha,\beta}^A(\omega) t_{\beta,b} \rho_{b,b}(\omega) t_{b,\beta} G_{\beta,\alpha}^R(\omega) t_{\alpha,a}, \end{aligned}$$

where $\hbar\omega$ is equal to the bias voltage energy eV ; $\rho_{a,a}(\omega)$ and $\rho_{b,b}(\omega)$ are the density of states in electrodes “a” and “b” at energy $\hbar\omega$; $t_a \equiv t_{a,\alpha} = t_{\alpha,a}$ and $t_b \equiv t_{b,\beta} = t_{\beta,b}$ are the hopping amplitudes for the contact with the points α and β at the extremities of the insulator to their counterparts a and b in the normal electrodes (see Figs. 3a for planar interfaces, and Fig. 3b for the 1D model¹). Eq. (21) is valid to all orders in the tunnel amplitudes t_a and t_b , from tunnel junctions to highly transparent interfaces. The fully dressed advanced and retarded Green’s functions $G_{\alpha,\beta}^A(\omega)$ and $G_{\beta,\alpha}^R(\omega)$ describe propagation from α to β and from β to α respectively while including all possible excursions in the normal electrodes, as opposed to the notations $g_{\alpha,\beta}^A(\omega)$ and $g_{\beta,\alpha}^R(\omega)$ restricted to electrodes isolated from each other, with $t_a = t_b = 0$. Physically, electron propagation across the insulator from electrode N_a at time τ_a to electrode N_b at time τ_b (corresponding to the advanced Green’s function $G_{\alpha,\beta}^A(\omega)$) occurs within the same process as propagation of a hole backwards in time from electrode N_b at time τ_b to electrode N_a at time τ_a (corresponding to the retarded Green’s function $G_{\beta,\alpha}^R(\omega)$). As we show, the electron and hole can bounce independently at both interfaces during a tunneling process, corresponding to contributions to the conductance of higher order in tunnel amplitudes. This amounts to evaluating a transition probability as the square of a transition amplitude, which

contains interference terms corresponding among others to weak localization-like subgap tunneling.

b. Expansion of the transport formula: Considering a geometry in which a quasi-1D ring made of a band insulator is connected to two normal electrodes (see Fig. 3c), the fully dressed advanced Green’s function $G_{\alpha,\beta}^A$ [see Eqs. (8) and (9) in Ref. 1]

$$G_{\alpha,\beta}^A = \frac{g_{\alpha,\beta}^A}{d_a^A d_b^A - (d_a')^A (d_b')^A}, \quad (22)$$

with $d_a^A = 1 - g_{\alpha,\alpha}^A t_{\alpha,a} g_{a,a}^A t_{a,\alpha}$ and $d_b^A = 1 - g_{\beta,\beta}^A t_{\beta,b} g_{b,b}^A t_{b,\beta}$, $(d_a')^A = g_{\beta,\alpha}^A t_{\beta,a} g_{a,a}^A t_{a,\alpha}$, $(d_b')^A = g_{\alpha,\beta}^A t_{\alpha,b} g_{b,b}^A t_{b,\beta}$, is expanded in multiple crossings of the ring:

$$\begin{aligned} G_{\alpha,\beta}^A = & \frac{g_{\alpha,\beta}^A}{d_a^A d_b^A} \\ & + \frac{(g_{\alpha,\beta}^A)^2 g_{\beta,\alpha}^A}{(d_a^A d_b^A)^2} (t_{\beta,b} g_{b,b}^A t_{b,\beta}) (t_{\alpha,a} g_{a,a}^A t_{a,\alpha}) + \dots \end{aligned} \quad (23)$$

The expansion in Eq. (23) is justified by the damping of the electron wave-functions in the insulator^{4,44}. Separating propagation from α to β along the upper and lower branches of the ring and including the phase factors related to the enclosed flux Φ , the combination of Eq. (21)-(23) to Eqs. (A2)-(A5) leads to dominant $h/2e$ oscillations of the conductance with the magnetic flux, and to a negative magnetoresistance at low field (see Fig. 3d). Similar features were obtained by Latyshev *et al.*⁶ in the experiments on CDWs (see the items 3. and 4. in the summary of experiments in the Introduction). The coincidence is explained in Sec. IV by the same underlying weak localization-like subgap tunneling processes for band insulators and CDWs.

2. Coupling to a momentum channel

Now, we note that propagation across the insulator defines a “tunnel” of cross section area ξ_0^2 , with $\xi_0 \sim a_0 \epsilon_F / \Delta$ the coherence length (a_0 is the lattice spacing and ϵ_F the Fermi energy). Such a narrow channel is compatible with the following additional assumption: the insulator (with the dispersion relation on Fig. 1) consists of linear 1D chains perpendicular to the interfaces. Electrons on the right and left branches (denoted by \underline{R} and \underline{L}) are taken into account according to Sec. II A. We deduce that the specific set of \underline{R} and \underline{L} labels on Fig. 4a does not contribute to the conductance once the summation over the Fermi oscillations in different channels is carried out. By contrast, branch crossing at the interfaces (see the \underline{R} and \underline{L} labels on Fig. 4b) contribute for a finite value to the conductance, and involve a transfer of $2k_F$ momentum from one interface to the other across the insulating electrode. In a quasi-1D geometry, electrons above the gap on the right branch (label \underline{R}) of the BCS-like dispersion relation (see Fig. 1) can propagate physically to

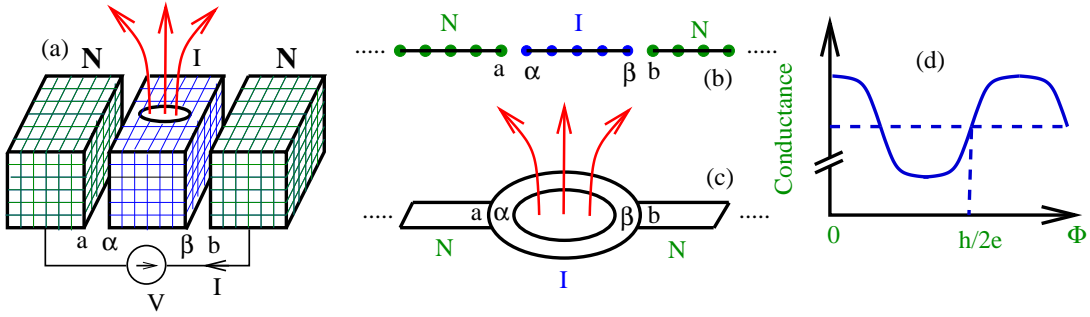


FIG. 3: (Color online.) Schematic representation of (a) a tight-binding normal metal - insulator - normal metal (NIN) tunnel junction with a hole pierced by a magnetic flux Φ in the insulator (b) the 1D NIN tunnel junction¹, and (c) a geometry with an insulating ring pierced by a flux Φ , and (d) the resulting $h/2e$ oscillations of the conductance with a negative magnetoresistance at low field. The notations a , α , β and b for labeling the interfaces are shown on the figure.

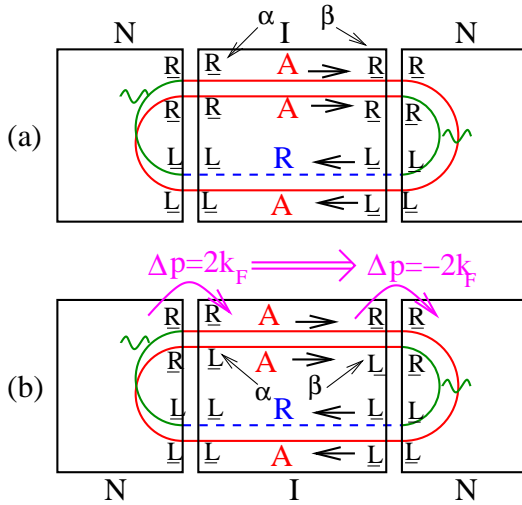


FIG. 4: (Color online.) Weak localization-like loops in a normal metal - insulator - normal metal junction with two sets of right-left labels. The right-left branches and therefore the momentum of the tunneling electrons is conserved in (a). The conductance is vanishingly small for (a) because of the absence of propagation from α to β of the advanced - advanced transmission mode ($g_{\alpha,\beta,\underline{R},\underline{R}}^A g_{\alpha,\beta,\underline{R},\underline{R}}^A \simeq 0$ for (a) - see Eq. (3)). (b) shows a process leading to a finite tunneling current ($g_{\alpha,\beta,\underline{R},\underline{R}}^A g_{\alpha,\beta,\underline{L},\underline{L}}^A$ is limited by the insulator coherence length for (b) - see Eq. (3)). Transfers of momentum by $\Delta p = \pm 2k_F$ propagate across the insulator according to the arrows, in parallel to evanescent wave charge tunneling.

the left or to the right according to their group velocity (see Fig. 1). This shows that a recoil of the insulator is a necessary condition for weak localization-like subgap tunneling. Moreover, transfers of $2k_F$ momentum are the hall-mark of CDW Andreev processes^{12,13,14}, which suggests a connection between the special type of tunnel junctions considered here and the CDW case (see Sec. IV). By comparison, a recoil of the insulator is not a necessary condition for the lowest order tunnel process in which an electron from the left normal electrode can be

transmitted in the insulator on the \underline{R} branch, and from the insulator to the right normal electrode.

Finally, disorder in the normal electrode tends to localize the electron wave functions in the vicinity of the interfaces. The processes on Fig. 4 are thus facilitated by a diffusive motion in the normal electrodes.

B. Subgap tunneling by a quantum interference effect in superconducting hybrids

1. Preliminaries on crossed transport in superconducting hybrids

Focusing now on similar effects in superconducting hybrids, we discuss subgap tunneling in a three-terminal normal metal - insulator - superconductor - insulator - normal metal (NISIN) trilayer under the form of crossed transport^{36,37,38}. The crossed conductance measures how the current $I_a(V_b)$ through the grounded electrode “a” responds to a voltage V_b on electrode “b” (see the electrical circuit on Fig. 5):

$$G_{a,b}(V_b) = \frac{\partial I_a}{\partial V_b}(V_b). \quad (24)$$

The crossed conductance^{36,37,38,39,40,41,42,43,44,45,46,47,48,49,50,56,57,58} given by Eq. (24) is either positive or negative^{36,37,38}, depending on whether the current $I_a(V_b)$ is dominated by normal transmission of electrons from electrode “b” to electrode “a” (the so-called “elastic cotunneling” channel) or by the anomalous transmission of electrons from electrode “b” to holes in electrode “a” with a pair left in the superconductor (the so-called “crossed Andreev reflection” channel). The later corresponds qualitatively to a splitting of entangled pairs from the superconductor in two different electrodes.

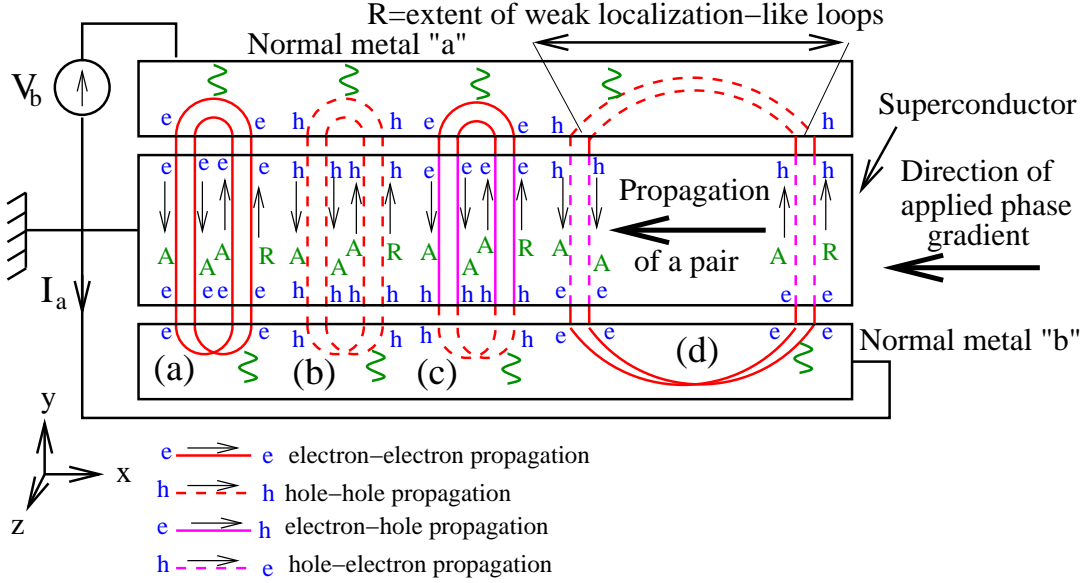


FIG. 5: (Color online.) Schematic representation of weak localization-like loops in crossed transport with specified electron (e) and hole (h) Nambu labels. The extent R of weak localization loops in the direction parallel to the layers is limited by the normal metal phase coherence length l_φ in the direction parallel to the layers⁴. The propagation of a pair (according to the arrows on (d)) between the two branches of the weak localization-like loop is involved for (c) and (d). (a) and (b) do not involve the propagation of a pair, and therefore do not couple to the phase gradient corresponding to a flow of supercurrent in the direction parallel to the layers.

2. Gauge transformation

Our goal here is to show in connection with Sec. III A that weak localization-like subgap tunneling involves a collective channel also in the superconducting case, analogous to the momentum channel for a tunnel junction.

Let us consider the trilayer geometry on Fig. 5, with a uniform phase gradient $\alpha = \partial\varphi(x)/\partial x$ along the x axis. We anticipate that the signature of the collective channel is provided by the coupling of the crossed conductance to a phase gradient α in the superconductor, because of the propagation of a pair in the direction parallel to the interfaces during the tunneling process (see Fig. 5d). Another contribution to the crossed conductance appearing to the same order in the interface transparency corresponds to double Andreev processes^{4,5}, which we do not discuss here.

The information on the superconducting phase gradient, initially contained in the Green's functions, is transferred to the hopping terms of the tight-binding Hamiltonian (see Eq. (4)) by a gauge transformation. The gauge transformed advanced Green's functions \tilde{G}_{x_1,x_2}^A encoding propagation from x_1 to x_2 is defined as $\tilde{G}_{x_1,x_2}^A = U_{x_1} G_{x_1,x_2}^A U_{x_2}^+$, with the diagonal matrix $\hat{U}_{x_1} = (\exp(-i\varphi(x_1)/2), \exp(i\varphi(x_1)/2))$, with a similar expression for \hat{U}_{x_2} , and where G_{x_1,x_2}^A is the Green's function without phase gradient. Going from wave-vectors to real space coordinates, the gauge transformed Green's function is shown to reduce to Eq. (6) without phase gradient in the relevant limit $\alpha a_0 \ll 1$, where a_0 is the tight bind-

ing lattice parameter. We use now $g_{x_1,x_2}^A = U_{x_1}^+ \tilde{g}_{x_1,x_2}^A U_{x_2}$, with \tilde{g}_{x_1,x_2}^A replaced by Eq. (6) to evaluate the weak localization-like diagrams, where the coupling to the superconducting phase gradient is all contained in $U_{x_1}^+$ and U_{x_2} .

3. Evaluation of the crossed conductance

We distinguish between two types of processes with long range propagation up to the phase coherence length l_φ in the normal electrodes in the direction parallel to the interfaces (see the detailed discussion of related processes in Ref. 4). First, a weak localization-like process with only normal electron-electron propagation (Figs. 5a and b) does not couple to the gradient of the superconducting phase variable. Second, the weak localization-like processes involving anomalous electron-hole propagation (Figs. 5c and d) couple to a gradient of the superconducting phase variable because in this case a pair is transferred from one of the two ‘‘branches’’ of the weak localization-like diagram to the other (see Fig. 5d). The crossed conductance is obtained from summing the four diagrams on Figs. 5a, b, c and d:

$$\mathcal{G}_{a,b}(V_b) = \mathcal{G}_{a,b}^{(0)}(V_b) \times [2 - \exp(2i(\varphi - \varphi')) - \exp(-2i(\varphi - \varphi'))], \quad (25)$$

where $\mathcal{G}_{a,b}^{(0)}(V_b) > 0$ according to Ref. 4, and where φ and $\varphi' = \varphi + \alpha R$ are the values of the superconducting variables at the places where the two branches of the weak

localization loops traverse the superconductor, within a distance R in the direction of the layers (see Fig. 5). Eq. (25) reduces to the crossed conductance

$$\mathcal{G}_{a,b}(V_b) = 4\mathcal{G}_{a,b}^{(0)}(V_b) \sin^2(\varphi - \varphi') \quad (26)$$

dominated by the crossed Andreev reflection channel. Eq. (26) leads to $\mathcal{G}_{a,b}(V_b) = 0$ if $\varphi = \varphi'$ in the absence of phase gradient, in agreement with Ref. 4. We have thus shown that a collective channel is involved in weak localization-like subgap tunneling in three terminal NISIN trilayers, in the form of a propagation of a pair in the condensate. Now we determine whether weak localization-like subgap tunneling in CDWs involves the condensate as in NISIN trilayers, or looks like quasi-1D insulators.

IV. SUBGAP TUNNELING BY A QUANTUM INTERFERENCE EFFECT AROUND A NANOHOLE IN A CHARGE DENSITY WAVE

Now, we present our main result and show that weak localization-like subgap tunneling discussed above for tunnel junctions (Sec. III A) and superconductors (Sec. III B) leads to a quantum interference effect also in charge density waves explaining the experiment by Latyshev *et al.*⁶ on oscillations of the CDW current around a nanohole. Before discussing weak localization-like subgap tunneling in Sec. IV A, we provide in Sec. IV B a mechanism specific to CDWs of transport around a nanohole. The influence of the sliding motion on elastic cotunneling through a CDW is postponed for Sec. IV C and the disordered case is discussed in Appendix B.

A. Coupling between the sliding motion and weak localization-like subgap tunneling

1. Notations

The mechanism discussed now for CDW transport, based on weak localization-like subgap tunneling around a nanohole, holds for a few interrupted chains coupled by a transverse hopping t_{\perp} . From the point of view of notations, the interrupted chains are labeled by $k = 2, \dots, N - 1$, and are connected by transverse hopping terms to the two uninterrupted chains $k = 1$ on top and $k = N$ on bottom (see Fig. 6 for $N = 3$ and Fig. 2c for $N = 5$). Chains $k = 2, \dots, N - 1$ are interrupted at positions $x_0^{(k)}$ at the left of the nanohole, and at $x_1^{(k)}$ at the right of the nanohole (see $x_0^{(2)}$ and $x_1^{(2)}$ on Fig. 6d for a single interrupted chain).

2. Deceleration and acceleration of the sliding motion in interrupted chains

Assuming an overall sliding motion, the phase $\varphi_k(x, \tau)$ at position x along chains $k = 1$ and $k = N$ and time τ follows $\partial\varphi_k(x, \tau)/\partial\tau = \omega_0$, with ω_0 the sliding frequency, corresponding to the relation (see for instance Ref. 33)

$$j^{(k)}(x, \tau) = \frac{e}{\pi} \frac{\partial\varphi_k(x, \tau)}{\partial\tau} \quad (27)$$

between the CDW current and the time derivative of the CDW phase variable in chain k . The boundary condition on the hole leads to $\partial\varphi_k(x, \tau)/\partial\tau = 0$ at $x = x_i^{(k)}$ ($i = 0, 1$ and $k = 2, \dots, N - 1$) (no collective current is flowing across $x_0^{(k)}$ and $x_1^{(k)}$ in the direction parallel to the chains), and to $\partial\varphi_k(x, \tau)/\partial\tau = \omega_0$ for $x \ll x_0^{(k)}$ and $x \gg x_1^{(k)}$ (the collective sliding motion is recovered far away from the nanohole). The resulting profile of $\partial\varphi_k(x, \tau)/\partial\tau$ (see Fig. 6c for $N = 3$) corresponds to the conversion of the CDW current in a normal current^{62,63,64,65} $\partial\rho_k(x, \tau)/\partial\tau$, emitted according to the arrows on Fig. 6b, from the intermediate chain labeled by k :

$$\frac{\partial\rho_k(x_0^{(k)}, \tau)}{\partial\tau} = -\frac{e}{\pi} \frac{\partial^2\varphi_k(x_0^{(k)}, \tau)}{\partial x\partial\tau}, \quad (28)$$

as deduced from the continuity equation.

3. Charge accumulation

Quasiparticles emitted from the slowing down of the sliding motion at the left of the nanohole are reabsorbed at its right where the sliding motion accelerates, leading to charge accumulation at the extremities of the interrupted chains at the left of the hole, described by a chemical potential $\delta\mu \gtrsim \Delta$. The current $I_k(\Phi)$ emitted from chain k is given by

$$I_k(\Phi) = \frac{e}{h} \sum_m \int_0^{\delta\mu} \mathcal{T}_{k \rightarrow m}(\Phi, t_{\perp}, \hbar\omega) d(\hbar\omega), \quad (29)$$

where $\mathcal{T}_{k \rightarrow m}(\Phi, t_{\perp}, \hbar\omega)$ is the total dimensionless transmission coefficient at energy $\hbar\omega$ transferring electrons from chain k at the left of the nanohole to chain m at its right (see chains k and m on Fig. 2). The subgap tunneling current is $h/2e$ -periodic as a function of the enclosed flux Φ (item 3. in the Introduction), as seen from the discussion of a normal tunnel junction in Sec. III A. The oscillations appear only in the presence of the sliding motion (item 2. in the Introduction). The smallness of interchain couplings in the transmission coefficient can be balanced by the integral over energy in Eq. (29), up to the large value of the Peierls gap in the compound NbSe₃ used by Latyshev *et al.*⁶. The non modulated part of the current for a single interrupted chain is proportional to

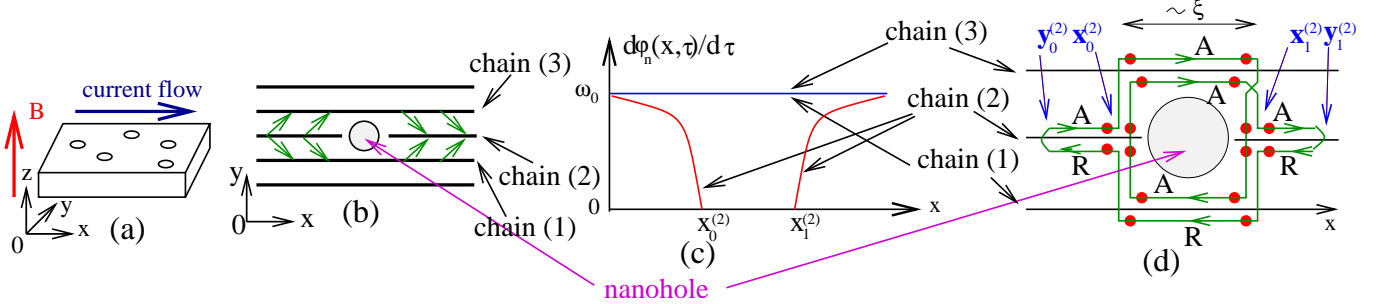


FIG. 6: (Color online.) Schematic representation of (a) a film of NbSe_3 pierced by nanoholes with a magnetic field \mathbf{B} along the z axis. The current is supposed to flow on average along the x axis parallel to the chains. (b) shows a nanohole interrupting a single CDW chain along the x axis. The arrows on (b) represent schematically the emission and absorption of normal carriers due to the slowing down and acceleration of the sliding motion at the left and right of the nanohole respectively. The profile of $d\varphi_n(x, \tau)/d\tau$ along chains $n = 1, 2, 3$ is shown schematically on (c) while (d) shows the same weak localization-like tunneling process as on Fig. 2c.

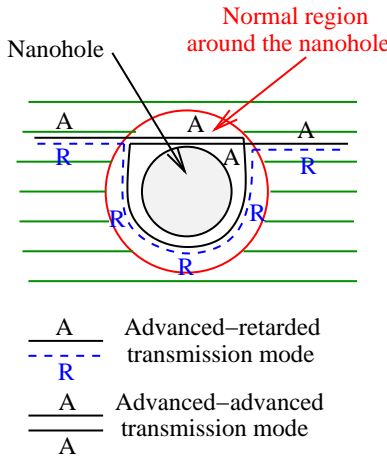


FIG. 7: (Color online.) Schematic representation of a weak localization-like tunneling events involving an “advanced-advanced” transmission mode, and an “advanced-retarded” transmission mode in the presence of a normal region around the nanohole, at energies smaller than the island level spacing.

$I_0 \sim (e/h)(t_\perp/T)^4(\delta\mu - \Delta)$ while the modulated part $I_{\text{mod}} = (e/h)(t_\perp/T)^8\Delta$ is independent on $\delta\mu - \Delta$. The ratio $I_{\text{mod}}/I_0 = (t_\perp/T)^4\Delta/(\delta\mu - \Delta)$ is thus expected to be small if $\delta\mu \gtrsim \Delta$. However, it was already noticed¹⁵ that the damaged region of the CDW around a nanohole may be normal. The corresponding tunneling process is shown on Fig. 7 at an energy smaller than the normal region level spacing δ . Propagation across the normal region supports “advanced-advanced” transmission modes because the level spacing δ plays the role of a gap. The value of δ is comparable to the Peierls gap, as it can be seen from the estimate $\hbar v_F/D$, with D the diameter of the nanohole, leading to the rough estimate $\delta/k_B \sim 100 \text{ K}$, with $v_F \simeq 10^5 \text{ ms}^{-1}$ as an order of magnitude of the Fermi velocity. As expected, the level spacing of an object of size $D \sim \xi$ is comparable to the Peierls gap Δ . Finally, the normal island may be disordered and

weak localization loops as on Fig. 6a may be possible. However, weak localization loops containing “advanced-advanced” diffusion modes are also possible because of scattering on disorder⁵, and their total contribution is much larger than weak localization loops with short range “advanced-advanced” propagation as on Fig. 6a.

B. Weak localization-like subgap tunneling transmission coefficient

We evaluate now the weak localization-like subgap tunneling transmission coefficient given by the diagram on Fig. 6d, in the absence of normal region around the nanohole as on Fig. 7. It takes the form

$$\mathcal{T}(\Phi = 0, t_\perp, \hbar\omega) = \left(\frac{t_\perp}{T}\right)^8 \mathcal{F}(\hbar\omega) \Xi(\hbar\omega), \quad (30)$$

where we suppose no applied magnetic flux. The factor $\Xi(\hbar\omega)$ encodes the damping of subgap transmission:

$$\Xi(\hbar\omega) = \exp\left(-\frac{y_1^{(2)} - y_0^{(2)}}{\xi(\omega)}\right) \exp\left(-\frac{x_1^{(2)} - x_0^{(2)}}{\xi(\omega)}\right), \quad (31)$$

and $\mathcal{F}(\hbar\omega)$ takes the form

$$\mathcal{F}(\hbar\omega) = \text{Re} \left[4 |g_0(\omega)|^4 \{ (g_0(\omega))^2 + (f_0(\omega))^2 \} \right. \quad (32) \\ \left. \times \{ |g_0(\omega)|^2 + |f_0(\omega)|^2 \} \right],$$

with $g_0(\omega)$ and $f_0(\omega)$ given by Eqs. (16) and (17). The term $|g_0(\omega)|^2 + |f_0(\omega)|^2$ corresponds to the “advanced-retarded” transmission mode in the lower branch (see Fig. 6d) and the term $(g_0(\omega))^2 + (f_0(\omega))^2$ accounts for the “advanced-advanced” transmission mode in the upper branch. The later involves a transmission of momentum in parallel to evanescent wave tunneling, similarly to the tunnel junction discussed in Sec. III A (see

Fig. 4b). The coherence length $\xi(\omega)$ at energy $\hbar\omega$ is given by $\xi(\omega) = \hbar v_F / \sqrt{|\Delta|^2 - (\hbar\omega)^2}$, with v_F the Fermi velocity.

The sliding motion induces a time dephasing of weak localization-like tunneling because the CDW phase evolves in time in the course of weak localization winding. On the other hand, the same effect induces already a coupling of elastic cotunneling to the sliding motion (see Sec. IV C). Such couplings are however not probed in experiments such as in Ref. 6 because the sliding motion is slow compared to the time scale \hbar/Δ , with Δ the Peierls gap (see Sec. IV C).

A ballistic evaluation of the transmission coefficient in the CDW chains (see Figs. 6d and Fig. 7b) is justified by the fact that tunneling quasiparticles travel over extremely short distances corresponding to the diameter of the hole, comparable to the CDW coherence length of order 10 nm in experiments⁶. Similar results were obtained in a different limit by treating disorder in the ladder approximation along Ref. 61 (the principle of the calculation is detailed in Appendix B).

C. Elastic cotunneling through a sliding charge density wave

To conclude, we evaluate now the direct coupling to the sliding motion for elastic cotunneling processes that contribute to the part of the tunneling current not modulated by a magnetic field (see Fig. 2d), and show that this coupling can be neglected as we did in Sec. IV B. We consider in this section such processes in a $N_a/CDW/N_b$ junction where a normal electron from site “a” in a normal electrode N_a enters a sliding CDW chain at site “ α ”, propagates within a sliding chain as a subgap quasiparticle up to site “ β ” over a distance $R_{\alpha,\beta}$ and exits to the other normal electrode N_b by jumping from site “ β ” to site “b”.

The tunneling current $I(V, \tau)$ at time τ for a voltage difference V is given by^{1,66}

$$I(V, \tau) = \frac{ie}{\hbar} \text{Tr} \left[\hat{t}_{a,\alpha} \hat{G}_{\alpha,a}^+(\tau, \tau) - \hat{t}_{\alpha,a} \hat{G}_{a,\alpha}^+(\tau, \tau) \right], \quad (33)$$

with $\hat{t}_{a,\alpha}$ ($\hat{t}_{\alpha,a}$) the hopping amplitudes matrices from site a to site α , (from site α to site a respectively), with the Keldysh Green’s function $\hat{G}_{x,y,j,k}^+(\tau, \tau') = i \langle c_{x,j}^+(\tau) c_{y,k}(\tau') \rangle$, with $x, y = a, \alpha$, and where the trace is a sum over the matrix element labels $j, k = \underline{R}, \underline{L}$ for right- and left-moving electrons. The operators $c_{x,j}^+(\tau)$ and $c_{x,j}(\tau)$ create and destroy respectively a $j = \underline{R}, \underline{L}$ moving fermion at position x and time τ .

The current $I(V, \tau)$ through a sliding CDW to lowest order in the tunnel amplitude, is such that

$$\frac{\partial I}{\partial V}(V) = 4\pi^2 \frac{e^2}{\hbar} \int \prod_{i=1}^4 d\tau_i \text{Tr} \left\{ \check{g}_{\alpha,\beta}^R(\tau_1, \tau_2) \right.$$

$$\left. \hat{U}_\beta(\tau_2) \hat{t}_{\beta,b} \hat{\rho}_{b,b} \left[\frac{\partial}{\partial V} n_F^b(\tau_2 - \tau_3) \right] \hat{t}_{b,\beta} \hat{U}_\beta^+(\tau_3) \right.$$

$$\left. \check{g}_{\beta,\alpha}^A(\tau_3 - \tau_4) \hat{U}_\alpha(\tau_4) \hat{t}_{\alpha,a} \hat{\rho}_{a,a} \hat{t}_{a,\alpha} \hat{U}_\alpha^+(\tau_4) \right\}, \quad (34)$$

where $t_a \equiv t_{a,\alpha} = t_{\alpha,a}$ and $t_b \equiv t_{b,\beta} = t_{\beta,b}$ are the hopping amplitudes at the interfaces $a-\alpha$ and $b-\beta$, τ_i ($i = 1, \dots, 4$) denote time variables, $\rho_{a,a}$ and $\rho_{b,b}$ correspond to the density of states in the normal electrodes N_a and N_b . The trace in Eq. (34) is a summation over the right-left components. We absorbed the sliding motion at frequency ω_0 in the gauge transformation $\hat{g}_{\alpha_1,\alpha_2}(\tau_1, \tau_2) = \hat{U}_\alpha(\tau_1) \check{g}_{\alpha_1,\alpha_2}(\tau_1, \tau_2) \hat{U}_\alpha^+(\tau_2)$ to a frame in which the CDW is static, where $\hat{U}_\alpha(\tau)$ and $\hat{U}_\beta(\tau)$ are diagonal matrices with elements $(\exp(i\omega_0\tau/2), \exp(-i\omega_0\tau/2))$. The notation $n_F^b(\tau_2 - \tau_3)$ in Eq. (34) stands for the Fourier transport from frequency to time variables of the Fermi distribution function in electrode N_b , and $\hat{g}_{\alpha,\beta}(\tau_\alpha, \tau_\beta)$ denotes a time-dependent Green’s function. We obtain

$$\frac{\partial I}{\partial V}(V) = 4\pi^2 \frac{e^2}{\hbar} t_a^2 t_b^2 \rho_N^2 \left\{ g_0 \left(\frac{eV}{\hbar} + \omega_0 \right) \right. \quad (35)$$

$$\left. \times g_0 \left(\frac{eV}{\hbar} + \omega_0 \right) + g_0 \left(\frac{eV}{\hbar} - \omega_0 \right) g_0 \left(\frac{eV}{\hbar} - \omega_0 \right) \right\}.$$

where $g_0(\omega)$ is given by Eq. (16), and where ρ_N is the density of states in the normal probes. We conclude that the sliding motion couples to elastic cotunneling by a shift of the energy $\hbar\omega$ by $\pm\hbar\omega_0$. However, in experiments, $\hbar\omega_0$ is much smaller than typical values of $\hbar\omega$, so that the CDW can be considered as static on the scale of subgap tunneling.

V. CONCLUSIONS

To conclude, we discussed a mechanism of tunneling by a quantum interference effect initially proposed for superconducting hybrids^{4,5,51}. We have shown that the generic features of this process is a coupling to an additional channel in parallel to evanescent quasiparticle tunneling, which occurs already for a model system provided by a specific tunnel junction, as well as in superconductors and CDWs. The detailed mechanisms by which weak localization-like tunneling enters transport properties differ from one system to the other, due to different dimensionalities and different relations between the current and the phase variable.

The considered tunneling mechanism combined to charge accumulation due to the deceleration of the CDW at the approach of the nanohole leads to the same features as in the experiment by Latyshev *et al.*⁶ on $h/2e$ oscillations of the CDW current around a nanohole (see the Introduction): 1. Weak localization-like loops due to higher order terms in the tunnel amplitudes are present even without nanoholes. They induce no oscillations in the magnetoresistance in the absence of nanohole because of the absence of charge accumulation in this case; 2. No

charge accumulation is present with nanoholes but without sliding motion; 3. $h/2e$ -periodic oscillations of the resistance as a function of the magnetic flux are obtained with nanoholes and with sliding motion because the diameter of the nanohole is comparable to the coherence length, so that weak localization-like loops enclose approximately the same area as the nanohole; 4. The positive magnetoresistance at low field is already obtained for the normal tunnel junction corresponding to Fig. 6d; 5. For Fig. 6c, the only energy/temperature scale in weak localization-like subgap tunneling is the Peierls gap. For Fig. 7, the characteristic energy/temperature is the level spacing of the metallic island, comparable to the Peierls gap.

An underlying question is whether the experiment by Latyshev *et al.*⁶ provides evidence for an interference effect associated to the collective quantum mechanical CDW ground state. The collective momentum channel is realized by a recoil of a quasi-1D insulator, as opposed to being mediated by the propagation of pairs in the condensate for superconducting hybrids. The analogy between CDWs and quasi-1D insulators and on the other hand the presence of a normal island shows that propagation through the CDW condensate is not a necessary condition for the modulations of the resistance as a function of a magnetic field.

Acknowledgments

R.M. thanks Yu. Latyshev, P. Monceau and A.A. Sinchenko for stimulating discussions on their experiments, S. Brazovski for a crucial discussion at the early stages of this work, and acknowledges a fruitful discussion with D. Carpentier and E. Orignac, as well as with J. Dumas. S. D. and R. M. thank D. Feinberg, S. Florens, M. Houzet and R. Whitney for having provided useful insights and suggestions. Ref. 51 was provided by M.V. Feigelman.

APPENDIX A: TUNNELING THROUGH AN INSULATOR WITH PLANAR INTERFACES

1. Multichannel transport formula

The exact generalization of the 1D transport formula (see Eq. (21)) to a multichannel N_aIN_b tunnel junction with extended interfaces (see Fig. 3a) is given by

$$\mathcal{G}(\omega) = \sum_{i,j,k,l} 4\pi^2 \frac{e^2}{h} \rho_{a_i, a_j}(\omega) t_{a_j, \alpha_j} G_{\alpha_j, \beta_k}^A(\omega) t_{\beta_k, b_k} \times \rho_{b_k, b_l}(\omega) t_{b_l, \beta_l} G_{\beta_l, \alpha_i}^R(\omega) t_{\alpha_i, a_i}, \quad (A1)$$

where an underlying tight-binding lattice is assumed. The density of states ρ_{a_i, a_j} connects the two sites a_i and a_j at the same interface. The summations over (i, j) and

(k, l) run over all sites at the N_aI and IN_b interfaces respectively. The transport formula given by Eq. (A1) is represented on Fig. 8a, where the bold red and dashed blue lines correspond to $G_{\alpha, \beta}^A$ and $G_{\beta, \alpha}^R$ respectively. The densities of states in the normal electrodes are represented by the connection of a wavy line on the figure.

2. Perturbative expansion

Higher order tunnel processes containing weak localization-like contributions are obtained by expanding systematically Eq. (A1) in the tunnel amplitudes according to the Dyson equations. Fig. 8 b-f shows combinations of some terms in $G_{\alpha, \beta}^A$ to some terms in $G_{\beta, \alpha}^R$. The weak localization-like diagrams on Fig. 8d and e are made of three “advanced” and one “retarded” Green’s functions, and look similar to the diagram on Fig. 2b corresponding to a disorder self-energy in the bulk of a superconductor.

3. Averaging over the conduction channels

The diagrams appearing in perturbation theory are averaged over the different “channels” in real space, corresponding to a summation over the discrete tight-binding sites at which diagrams cross the interfaces. The result of the channel averaging procedure depends on assumptions about the insulator band structure.

Averaging over the conduction channels amounts to evaluating the integrals

$$g^A(R_{\alpha, \beta}, \omega) g^R(R_{\alpha, \beta}, \omega) \quad (A2)$$

$$= \frac{k_F}{2\pi} \int_{R_{\alpha, \beta}}^{R_{\alpha, \beta} + 2\pi/k_F} g^A(r, \omega) g^R(r, \omega) dr \quad (A3)$$

$$= \frac{1}{2} \left(\frac{\pi \rho_N}{k_F R_{\alpha, \beta}} \right)^2 \frac{(\hbar\omega)^2}{|\Delta|^2 - (\hbar\omega)^2} \exp \left(-\frac{2R_{\alpha, \beta}}{\xi(\omega)} \right) \quad (A4)$$

$$= \overline{g^A(R_{\alpha, \beta}, \omega) g^A(R_{\alpha, \beta}, \omega)}, \quad (A5)$$

where $g^A(R_{\alpha, \beta}, \omega)$ is given by Eq. (1), and where the last equality is valid for $\hbar\omega < \Delta$ below the gap. To summarize, Aharonov-Bohm like oscillations are washed out by channel averaging with the band structure on Fig. 1 and $h/2e$ -periodic weak localization-like diagrams on Figs. 8d and e contribute to leading order (in the tunnel amplitudes) to the oscillations of the conductance as a function of the magnetic flux.

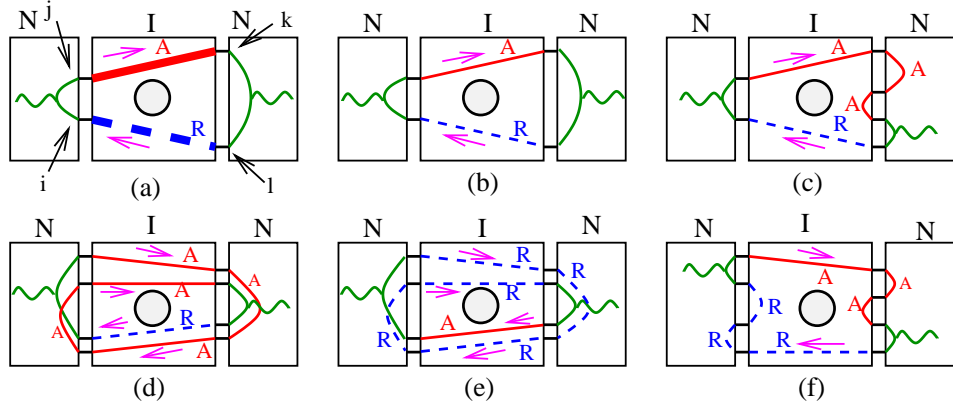


FIG. 8: (Color online.) Top view of Fig. 3a showing the first terms in perturbation theory in the tunnel amplitude for a normal metal - insulator - normal metal (NIN) tunnel junction. The exact transport formula is shown schematically on (a), where the thick solid (dashed) lines correspond to the fully dressed advanced (retarded) Green's functions. The wavy lines indicate the insertion of the density of states in the normal electrodes (see Fig. 3b). The other panels correspond to some low order terms in the perturbative expansion in the tunnel amplitudes. As for usual weak localization in a normal metal (see Fig. 2a), the weak localization-like tunneling processes on (d) and (e) lead to dominant $h/2e$ oscillations as a function of the magnetic flux once the summation over all channels has been carried out.

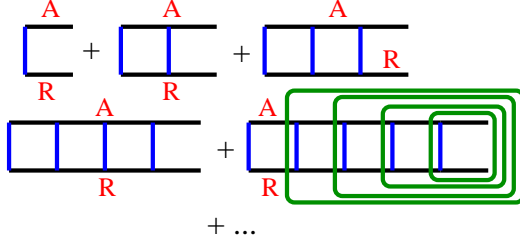


FIG. 9: (Color online.) The ladder series for the transmission coefficient. The vertical blue lines correspond to impurities in the ladder approximation. The green boxes corresponding to Eq. (B5) indicate the recursive elimination of the impurities from one extremity of the ladder⁶¹.

APPENDIX B: EVALUATION OF THE TRANSMISSION COEFFICIENT OF A DISORDERED CDW

1. Green's function of a disordered CDW

The Green's function of a disordered CDW is evaluated in the Born approximation as in the superconducting case, where we introduce forward- and backward-scattering potentials u and v . With the notation in Ref. 61 in the superconducting case, we find

$$\hat{G}(\xi, \omega) = \frac{\hbar\omega + \bar{\xi}\hat{\tau}_3 + \bar{\Delta}\hat{\tau}_1}{(\hbar\omega)^2 - \bar{\xi}^2 - \bar{\Delta}^2}, \quad (\text{B1})$$

with $\hat{\tau}_1$ and $\hat{\tau}_3$ the Pauli matrices given below, with $\bar{\omega} = \omega(1 + \alpha)$, $\bar{\xi} = \xi + \beta$ and $\bar{\Delta} = \Delta(1 + \gamma)$, with

$$\alpha = \frac{1}{\tau_f \sqrt{\Delta^2 - \omega^2}} + \frac{1}{\tau_b \sqrt{\Delta^2 - \omega^2}} \quad (\text{B2})$$

$$= -(|u|^2 + |v|^2) \int \lambda_F \frac{dk}{2\pi} \frac{1}{(\hbar\omega)^2 - \Delta^2 - \xi^2} \quad (\text{B3})$$

$$\beta = \frac{1}{\tau_f \sqrt{\Delta^2 - (\hbar\omega)^2}} \quad (\text{B4})$$

$$= |u|^2 \int \lambda_F \frac{dk}{2\pi} \frac{1}{(\hbar\omega)^2 - \Delta^2 - \xi^2},$$

where λ_F is the Fermi wave-vector, $\hbar\omega$ the energy, Δ the CDW gap and ξ the kinetic energy with respect to the Fermi level. The notations τ_f and τ_b stand for the forward and backward scattering times respectively. We keep in the following calculations a finite shift β of the chemical potential that does however not enter the properties that we consider.

2. Evaluation of ladder diagrams for the transmission coefficient

To include disorder⁶⁷, the transmission coefficients in the ladder approximation are evaluated here according to Smith and Ambegaokar⁶¹ by iterations of

$$\hat{F}(\hat{\tau}_n) = \int \frac{dk}{2\pi} \left(\begin{array}{cc} u & w \\ v & u \end{array} \right)^\dagger \hat{G}^A(k, \omega) \hat{\tau}_n \hat{G}^R(k + q, \omega) \left(\begin{array}{cc} u & w \\ v & u \end{array} \right), \quad (\text{B5})$$

where u , v and w are Gaussian distributed random variable. The Pauli matrices $\hat{\tau}_n$ are such that

$$\hat{\tau}_0 = \left(\begin{array}{cc} 1 & 0 \\ 0 & 1 \end{array} \right), \quad \hat{\tau}_1 = \left(\begin{array}{cc} 0 & 1 \\ 1 & 0 \end{array} \right) \quad (\text{B6})$$

$$i\hat{\tau}_2 = \left(\begin{array}{cc} 0 & 1 \\ -1 & 0 \end{array} \right), \quad \hat{\tau}_3 = \left(\begin{array}{cc} 1 & 0 \\ 0 & -1 \end{array} \right). \quad (\text{B7})$$

We find

$$\begin{aligned}\hat{F}(\hat{\tau}_0) &= (-A + B)(1 - \alpha)\hbar\omega\hat{\tau}_3 \\ &\quad - 3A(1 + \gamma)\Delta i\hat{\tau}_2\end{aligned}\quad (\text{B8})$$

$$\begin{aligned}\hat{F}(\hat{\tau}_1) &= (A - B)(1 + \gamma)\Delta\hat{\tau}_3 \\ &\quad - 3A(1 - \alpha)\hbar\omega i\hat{\tau}_2\end{aligned}\quad (\text{B9})$$

$$\begin{aligned}\hat{F}(i\hat{\tau}_2) &= 3(A + B)(1 + \gamma)\Delta\hat{\tau}_0 \\ &\quad - 3A(1 - \alpha)\hbar\omega\hat{\tau}_1\end{aligned}\quad (\text{B10})$$

$$\begin{aligned}\hat{F}(\hat{\tau}_3) &= (-A - B)(1 - \alpha)\hbar\omega\hat{\tau}_0 \\ &\quad - A(1 + \gamma)\Delta\hat{\tau}_1,\end{aligned}\quad (\text{B11})$$

with

$$A = \frac{m^2}{4\hbar^4 k_F^5} \frac{(8k_F^2 + 19q^2)|u|^2}{(\Delta^2(1 + \gamma)^2 - \hbar\omega^2(1 - \alpha)^2)^{1/2}} \quad (\text{B12})$$

$$B = \frac{m^2}{4\hbar^4 k_F^5} \frac{(8k_F^2 + 19q^2)|v|^2}{(\Delta^2(1 + \gamma)^2 - \hbar\omega^2(1 - \alpha)^2)^{1/2}} \quad (\text{B13})$$

$$\cdot \quad (\text{B14})$$

Acting twice with \hat{F} according to $\hat{G} = \hat{F}^2$ leads to the closed 2×2 equations

$$\hat{G} \begin{pmatrix} \hat{\tau}_0 \\ \hat{\tau}_1 \end{pmatrix} = \begin{pmatrix} a & b \\ b' & a' \end{pmatrix} \begin{pmatrix} \hat{\tau}_0 \\ \hat{\tau}_1 \end{pmatrix} \quad (\text{B15})$$

$$\hat{G} \begin{pmatrix} i\hat{\tau}_2 \\ \hat{\tau}_3 \end{pmatrix} = \begin{pmatrix} c & d \\ d' & c' \end{pmatrix} \begin{pmatrix} i\hat{\tau}_2 \\ \hat{\tau}_3 \end{pmatrix}, \quad (\text{B16})$$

with

$$\begin{aligned}a &= (A^2 - B^2)(1 - \alpha)^2(\hbar\omega)^2 \\ &\quad - 9A(A + B)(1 + \gamma)^2\Delta^2\end{aligned}\quad (\text{B17})$$

$$b = A(10A - B)(1 - \alpha)(1 + \gamma)\hbar\omega\Delta \quad (\text{B18})$$

$$\begin{aligned}b' &= -(A + B)(10A - B)(1 - \alpha)(1 + \gamma) \\ &\quad \times \hbar\omega\Delta\end{aligned}\quad (\text{B19})$$

$$\begin{aligned}a' &= 9A^2(1 - \alpha)^2(\hbar\omega)^2 \\ &\quad - A(A - B)(1 + \gamma)^2\Delta^2,\end{aligned}\quad (\text{B20})$$

and expressions of the same type for c, d, c', d' :

$$c = -3(A - B)(2A + B)(1 - \alpha)(1 + \gamma) \quad (\text{B21})$$

$$\times \hbar\omega\Delta$$

$$\begin{aligned}d &= -9A[(A + B)(1 + \gamma)^2\Delta^2 \\ &\quad - A(1 - \alpha)^2(\hbar\omega)^2]\end{aligned}\quad (\text{B22})$$

$$\begin{aligned}c' &= (A - B)[(A + B)(1 - \alpha)^2(\hbar\omega)^2 \\ &\quad - A(1 + \gamma)^2\Delta^2]\end{aligned}\quad (\text{B23})$$

$$d' = 3A(2A + B)(1 - \alpha)(1 + \gamma)\hbar\omega\Delta. \quad (\text{B24})$$

The final step is to decompose the initial condition on the eigenvectors of \hat{G} and evaluate the coefficients in matrix geometric series such as

$$\sum_{n=1}^{+\infty} \hat{G}^n \begin{pmatrix} \hat{\tau}_0 \\ 0 \end{pmatrix} = A_1 \begin{pmatrix} \hat{\tau}_0 \\ 0 \end{pmatrix} + B_1 \begin{pmatrix} 0 \\ \hat{\tau}_1 \end{pmatrix} \quad (\text{B25})$$

$$\sum_{n=1}^{+\infty} \hat{G}^n \begin{pmatrix} 0 \\ \hat{\tau}_1 \end{pmatrix} = A_2 \begin{pmatrix} \hat{\tau}_0 \\ 0 \end{pmatrix} + B_2 \begin{pmatrix} 0 \\ \hat{\tau}_1 \end{pmatrix} \quad (\text{B26})$$

We find

$$A_1 = X \frac{\lambda_+}{1 - \lambda_+} \psi_+^{(1)} + Y \frac{\lambda_-}{1 - \lambda_-} \psi_-^{(1)} \quad (\text{B27})$$

$$B_1 = X \frac{\lambda_+}{1 - \lambda_+} \psi_+^{(2)} + Y \frac{\lambda_-}{1 - \lambda_-} \psi_-^{(2)} \quad (\text{B28})$$

$$A_2 = -X' \frac{\lambda_+}{1 - \lambda_+} \psi_+^{(1)} + X' \frac{\lambda_-}{1 - \lambda_-} \psi_-^{(1)} \quad (\text{B29})$$

$$B_2 = -X' \frac{\lambda_+}{1 - \lambda_+} \psi_+^{(2)} + X' \frac{\lambda_-}{1 - \lambda_-} \psi_-^{(2)}, \quad (\text{B30})$$

with

$$X = \frac{1}{2} \left(1 - \frac{b' - a}{(b' - a)^2 + 4a'b} \right) \quad (\text{B31})$$

$$Y = \frac{1}{2} \left(1 + \frac{b' - a}{(b' - a)^2 + 4a'b} \right) \quad (\text{B32})$$

$$X' = \frac{b}{(b' - a)^2 + 4a'b} \quad (\text{B33})$$

$$\lambda_{\pm} = \frac{1}{2} \left(a + b' \pm \sqrt{(a - b')^2 + 4a'b} \right) \quad (\text{B34})$$

$$\psi_{\pm}^{(2)} = \frac{b' - b \pm \sqrt{(a - b')^2 + 4a'b}}{2b} \quad (\text{B35})$$

and $\psi_{\pm}^{(1)} = 1$. Carrying out the same calculation in the sector $(i\hat{\tau}_2, \hat{\tau}_3)$ and evaluating geometric series like

$$\sum_{n=1}^{+\infty} \hat{G}^n \hat{F} \begin{pmatrix} \hat{\tau}_0 \\ 0 \end{pmatrix} \quad (\text{B36})$$

in both sectors leads to an expression of all right-left components of the transmission coefficient of a disordered CDW. The later can be used to evaluate the weak localization-like subgap tunneling diagrams.

¹ C. Caroli, R. Combescot, P. Nozières and D. Saint-James, J. Phys. C: Solid St. Phys. **4**, 916 (1971); *ibid.* **5**, 21 (1972).

² D.S. Golubev and A. Zaikin, Phys. Rev. B **74**, 245329 (2006).

³ Ya. M. Blanter, V.M. Vinokur, and L.I. Glazman, Phys. Rev. B **73**, 165322 (2006).

⁴ R. Mélin, Phys. Rev. B **73**, 174512 (2006).

⁵ S. Duhot and R. Mélin, Eur. Phys. J B **53**, 257 (2006); cond-mat/0610416.

⁶ Yu. I. Latyshev, O. Laborde, P. Monceau and S. Klaumünzer, Phys. Rev. Lett. **78**, 919 (1997).

⁷ *Charge Density Waves in Solids*, edited by L.P. Gor'kov and G. Grüner, Modern Problems in Condensed Matter Science Vol. 25 (North Holland, Amsterdam, 1989).

⁸ K.O'Neill, E. Slot, R. Thorne and H. van der Zant, J. Phys. IV France **131**, 221 (2005).

⁹ E. Slot, M.A. Holst, H.S.J. van der Zant, and S.V. Zaitsev-Zotov, Phys. Rev. Lett. **93**, 176602 (2004).

¹⁰ Yu. I. Latyshev, B. Pannetier and P. Monceau, Eur. Phys. J. B **3**, 421 (1998).

¹¹ Z.Z. Wang, J.C. Girard, C. Pasquier, D. Jérôme, and K. Bechgaard, Phys. Rev. B **67**, 121401 (2003).

¹² A.A. Sinchenko, Yu. I. Latyshev, S. G. Zybtshev, I. G. Gorlova, P. Monceau, Pis'ma Zh. Eksp. Teor. Fiz. **64**, 259 (1996) [JETP Lett. **64**, 285 (1996)]; A.A. Sinchenko, Yu. I. Latyshev, S. G. Zybtshev, I. G. Gorlova, Zh. Eksp. Teor. Fiz. **113**, 1830 (1998) [JETP **86**, 1001 (1998)]; Yu.I. Latyshev and A.A. Sinchenko, Pis'ma Zh. Eksp. Teor. Fiz. **75**, 714 (2002) [JETP Letters **75**, 593 (2002)].

¹³ A.L. Kasatkin and E.A. Pashitskii, Fiz. Nizk. Temp. **10**, 640 (1984); A.L. Kasatkin and E.A. Pashitskii, Fiz. Tverd. Tela (Leningrad) **27**, 2417 (1985) [Sov. Phys. Solid State **27**, 1448 (1985)].

¹⁴ S.N. Artemenko and S.V. Remizov, Pis'ma Zh. Eksp. Teor. Fiz. **65**, 50 (1997) [JETP Lett. **65**, 53 (1997)].

¹⁵ M.I. Visscher, B. Rejaei and G.E.W. Bauer, Phys. Rev. B **62**, 6873 (2000).

¹⁶ E.N. Bogachev, I.V. Krive, I.O. Kulik, and A.S. Rozhavsky, Phys. Rev. B **42**, 7614 (1990).

¹⁷ J.H. Miller, Jr., C. Ordóñez and E. Prodan, Phys. Rev. Lett. **84**, 1555 (2000).

¹⁸ G. Montambaux, Eur. Phys. J. B **1**, 377 (1998).

¹⁹ J. Yi, M.Y. Choi, K. Park, E.-H. Lee, Phys. Rev. Lett. **78**, 3523 (1997); N. Nathanson, O. Entin-Wohlman and B. Mühlischlegel, Phys. Rev. Lett. **80**, 3416 (1998); G. Montambaux, Phys. Rev. Lett. **80**, 3417 (1998).

²⁰ L.P. Gorkov, Pis'ma Zh. Eksp. Teor. Fiz. **38**, 76 (1983) [JETP Lett. **38**, 87 (1983)].

²¹ S.N. Artemenko and A.F. Volkov, in Ref. 7, Chap. 9.

²² S.A. Brazovskii, in Ref. 7, p. 425.

²³ S.A. Brazovskii and S.I. Matveenko, Zh. Eksp. Teor. Fiz. **99**, 1539 (1991) [Sov. Phys. JETP **72**, 860 (1991)].

²⁴ S. Ramakrishna, M.P. Maher, V. Ambegaokar and U. Eckern, Phys. Rev. Lett. **68**, 2066 (1992).

²⁵ M.P. Maher, T.L. Adelman, S. Ramakrishna, J.P. McCarten, D.A. DiCarlo and R.E. Thorne, Phys. Rev. Lett. **68n** 3084 (1992).

²⁶ T.L. Adelman, M.C. de Lind van Wijngaarden, S.V. Zaitsev-Zotov, D. DiCarlo and R.E. Thorne, Phys. Rev. B **53**, 1833 (1996).

²⁷ H. Requardt, F. Ya. Nad, P. Monceau, R. Currat, J.E. Lorenzo, S. Brazovskii, N. Kirova, G. Grübel and Ch. Vettier, Phys. Rev. Lett. **80**, 5631 (1998).

²⁸ N. Hatakenaka, M. Shiobara, K. Matsuda and S. Tanda, Phys. Rev. B **57**, R2003 (1998).

²⁹ Y. Takane, J. Phys. Soc. Jpn. **71**, 1019 (2002), **71**, 1824 (2002); Y. Takane and K. Wakabayashi, J. Phys. Soc. Jpn. **70**, 1869 (2001).

³⁰ N.P. Ong, G. Verma and K. Maki, Phys. Rev. Lett. **52**, 663 (1984).

³¹ S. Brazovskii, N. Kirova, H. Requardt, F. Ya. Nad, P. Monceau, R. Currat, J.E. Lorenzo, G. Grübel and Ch. Vettier, Phys. Rev. B **61**, 10640 (2000).

³² S.N. Artemenko, Phys. Rev. B **67**, 125420 (2003).

³³ S. Brazovskii and T. Nattermann, Advances in Physics **53**, 177 (2004).

³⁴ C.J. Lambert and R. Raimondi, J. Phys.: Condens. Matter **10**, 901 (1998).

³⁵ F.J. Jedema, B.J. van Wees, B.H. Hoving, A.T. Filip, and T.M. Klapwijk, Phys. Rev. B **60**, 16549 (1999).

³⁶ J. M. Byers and M. E. Flatté, Phys. Rev. Lett. **74**, 306 (1995).

³⁷ G. Deutscher and D. Feinberg, App. Phys. Lett. **76**, 487 (2000).

³⁸ G. Falci, D. Feinberg, and F.W.J. Hekking, Europhys. Lett. **54**, 255 (2001).

³⁹ P. Samuelsson, E. V. Sukhorukov, and M. Büttiker, Phys. Rev. Lett. **91**, 157002 (2003).

⁴⁰ E. Prada and F. Sols, Eur. Phys. J. B **40**, 379 (2004).

⁴¹ P.K. Polinák, C.J. Lambert, J. Kolai, and J. Cserti, Phys. Rev. B **74**, 132508 (2006).

⁴² T. Yamashita, S. Takahashi and S. Maekawa, Phys. Rev. B **68**, 174504 (2003).

⁴³ D. Feinberg, Eur. Phys. J. B **36**, 419 (2003).

⁴⁴ R. Mélin and D. Feinberg, Phys. Rev. B **70**, 174509 (2004).

⁴⁵ F. Giazotto, F. Taddei, F. Beltram and R. Fazio, Phys. Rev. Lett. **97**, 087001 (2006).

⁴⁶ S. Russo, M. Kroug, T.M. Klapwijk, and A.F. Morpugo, Phys. Rev. Lett. **95**, 027002 (2005).

⁴⁷ D. Beckmann, H.B. Weber, and H. v. Löhneysen, Phys. Rev. Lett. **93**, 197003 (2004). D. Beckmann and H. v. Löhneysen, LT 24 conference proceedings, cond-mat/0512445 (2005).

⁴⁸ P. Cadden-Zimansky and V. Chandrasekhar, cond-mat/0609749.

⁴⁹ M.S. Choi, C. Bruder, and D. Loss, Phys. Rev. B **62**, 13569 (2000); P. Recher, E. V. Sukhorukov, and D. Loss Phys. Rev. B **63**, 165314 (2001).

⁵⁰ G. B. Lesovik, T. Martin, and G. Blatter, Eur. Phys. J. B **24**, 287 (2001); N. M. Chtchelkatchev, G. Blatter, G. B. Lesovik, and T. Martin, Phys. Rev. B **66**, 161320(R) (2002).

⁵¹ A. Altland and M.R. Zirnbauer, Phys. Rev. B **55**, 1142 (1997).

⁵² S.N. Artemenko and A.F. Volkov, Zh. Éksp. Teor. Fiz. **81**, 1872 (1981) [Sov. Phys. JETP **53**, 1050 (1981)].

⁵³ R. Mélin and S. Peysson, Phys. Rev. B **68**, 174515 (2003).

⁵⁴ L.P. Gorkov, A. Larkin, and D.E. Khmelnitskii, Pis'ma Zh. Eksp. Teor. Fiz. **30**, 248 (1979) [JETP Lett. **30**, 228 (1979)].

⁵⁵ S. Hikami, Phys. Rev. B **24**, 2671 (1981).

⁵⁶ D. Sánchez, R. López, P. Samuelsson, and M. Büttiker, Phys. Rev. B **68**, 214501 (2003).

⁵⁷ M.S. Kalenkov and A.D. Zaikin, cond-mat/0611330.

⁵⁸ A. Brinkman and A.A. Golubov, cond-mat/0611144.

⁵⁹ J. P. Morten, A. Brataas and W. Belzig, cond-mat/0606561; J. P. Morten, D. Huertas-Hernando, A. Brataas, W. Belzig, cond-mat/0612197.

⁶⁰ A. Levy Yeyati, F.S. Bergeret, A. Martin-Rodero and T.M. Klapwijk, cond-mat/0612027.

⁶¹ R. A. Smith and V. Ambegaokar, Phys. Rev. B **45**, 2463

(1992).

⁶² Yu. I. Latyshev, P. Monceau, S. Brazovskii, A.P. Orlov, and T. Fournier, Phys. Rev. Lett. **96**, 116402 (2006).

⁶³ N. Kirova, S. Brazovskii, J. Physique IV **12** Pr9-173 (2002).

⁶⁴ D. Rideau, P. Monceau, R. Currat, H. Requardt, F. Nad, J.E. Lorenzo, S. Brazovskii, C. Detlefs, G. Grübel, Euro-phys. Lett. **56**, 289 (2001).

⁶⁵ S. Brazovskii, N. Kirova, H. Requardt, F. Ya. Nad, and P. Monceau, Phys. Rev. B **61**, 10640 (2000).

⁶⁶ J Dong, Commun. Theor. Phys. **11**, 231 (1989).

⁶⁷ A. Vanyolos, B. Dora, K. Maki, A. Virosztek, cond-mat/0606578.